Materials Today Advances 2 (2019) 100008

Contents lists available at ScienceDirect

Materials Today Advances

journal homepage: www.journals.elsevier.com/materials-today-advances/

Polymer nanocomposites functionalised with nanocrystals of zeolitic imidazolate frameworks as ethylene control agents

E.M. Mahdi [a, 1], C. Cuadrado-Collados [b, 1], J. Silvestre-Albero [b, **], Jin-Chong Tan [a, *]

[a] Multifunctional Materials & Composites (MMC) Laboratory, Department of Engineering Science, University of Oxford, Parks Road, OX1 3PJ, United Kingdom

[b] Laboratorio de Materiales Avanzados, Departamento de Química Inorgánica-Instituto Universitario de Materiales, Universidad de Alicante, Ctra. San Vicente-Alicante s/n, E-03080 Alicante, Spain

ARTICLE INFO

Article history:
Received 3 February 2019
Received in revised form
8 April 2019
Accepted 12 April 2019
Available online xxx

Keywords:
Mixed-matrix membranes
Dynamic framework structure
Adsorption–desorption kinetics
Gate opening
Polyurethane
Matrimid

ABSTRACT

Ethylene (C_2H_4) management involves the usage of materials such as $KMnO_4$ or processes such as ozone oxidation or combined photocatalysis/photochemistry. The ubiquity of C_2H_4, especially in an industrial context, necessitates a simpler and much more effective approach, and herein we propose the usage of tuneable polymer nanocomposites for the adsorption of C_2H_4 through the modification of the polymer matrices *via* the incorporation of nanocrystals of zeolitic imidazolate frameworks (nano-ZIFs). We demonstrate that the inclusion of ZIF-8 and ZIF-7 nanocrystals into polymeric matrices (Matrimid and polyurethane [PU]) yields robust nanocomposites that preserve the C_2H_4 adsorption/desorption capacity of nanocrystals while shielding it from degrading factors. We report new insights into the adsorption/desorption kinetics of the polymer and its corresponding nanocomposites, which can be tailored by exploiting the underlying polymeric molecular interactions. Importantly, we also elucidated the retention of the intrinsic structural framework dynamics of the nano-ZIFs even when embedded within the polymeric matrix, as evidenced from the breathing and gate-opening phenomena. Our findings pave the way for bespoke designs of novel polymer nanocomposites, which will subsequently impact the deployment of tailored nanomaterials for effective industrial applications.

1. Introduction

Commercially available approaches for ethylene (C_2H_4) management (for instance, in packaging applications for long-distance transportation of perishable produce such as fruits and vegetables [1,2]) are generally focussed on the removal of C_2H_4 or its conversion to benign molecules, e.g., *via* inhibition of C_2H_4 synthesis [3], absorption/adsorption using chemicals and/or catalysts [4] and photocatalytic and photochemical oxidation strategies [5]. Certain systems pertaining to the removal of C_2H_4 (e.g. UV photodecomposition and ozone degradation) are technically impractical on a large scale, either due to the production of undesired excess molecules or from its dismal efficiency at lower concentrations [6,7]. This necessitates the development of new approaches for C_2H_4 management under a range of concentrations and temperatures. A potential alternative scarcely explored in literature eschewing the use of complex removal techniques is the utilisation of porous sorbent minerals (deployed in the form of newly formed materials or composites) for C_2H_4 management. Traditional materials such as zeolites or inorganic oxides (e.g. TiO_2) have been embedded in polymeric matrices to engineer bespoke composite materials for this purpose [8]. However, the reported systems commonly cite problems pertaining to their limited adsorption capacity. One of the primary challenges in the design of these polymer-based composite systems is the proper integration of the adsorbents (fillers) while also preserving the adsorption performance of the fillers alongside the thermomechanical resilience of the resulting (nano)composites [9].

Amongst potential candidates as fillers, metal–organic frameworks (MOFs) exhibit key advantages such as an inherent porosity, specific aperture size and large surface areas (>1000 $m^2\ g^{-1}$), rendering them excellent for the capture/separation of a wide variety of gases, ranging from atmospheric ones (O_2, N_2, H_2 and CO_2) to hydrocarbons such as ethane (C_2H_6) and ethylene (C_2H_4)

* Corresponding author.
** Corresponding author.
E-mail addresses: joaquin.silvestre@ua.es (J. Silvestre-Albero), jin-chong.tan@eng.ox.ac.uk (J.-C. Tan).
[1] These authors have contributed equally to the results.

https://doi.org/10.1016/j.mtadv.2019.100008

[10–13]. Its viability is further enhanced by the fact that it is possible to produce bespoke MOFs that would respond to specific guest species *via* the tuning of its pore chemistry and size [14]. Zeolitic imidazolate frameworks (ZIFs) are a subclass of MOFs known for their superb combination of chemical and thermo-mechanical properties [15,16]. Recent studies reported that ZIFs have a high chemical affinity towards adsorption and capture/separation of light hydrocarbons (C_1-C_4 hydrocarbons) [17–19], and their adsorption capability is usually dictated by unique structural deformations such as the 'gate-opening' effect of ZIF-8 [20–23], or the 'breathing' phenomenon of the pore windows of ZIF-7, among others [22,24,25]. Gücüyener et al. [26] reported a promising adsorption capacity for light hydrocarbons in ZIF-7 (only methane was excluded from the inner porosity), achieving an olefin/paraffin selectivity value of 2.5, while Bux et al. [27] reported that membranes formed using ZIF-8 are capable of adsorbing olefin and paraffin, where the adsorption of the latter being more favourable (stronger adsorption) than that of the former. The higher selectivity of ZIF-8 *vis-à-vis* ethane over ethene was confirmed by Bohme et al. [28] with an adsorption capacity of ~1.5 mmol g^{-1} and 2.5 mmol g^{-1} for ethene and ethane, respectively, at 1 bar and 25 °C (298 K). It is therefore reasoned that the excellent ability of ZIFs in general to capture and separate hydrocarbons would also extend to its corresponding composites if its polymer matrix does not impede the functionality of the pristine ZIF fillers.

Exploring the usage of ZIFs for gas capture and separation has been a continuous endeavour alongside the recent development of ZIF-based composites [29] and more generally of polymer nanocomposites incorporating MOF fillers [30,31]. It can also be argued that the advent of ZIF-based composites further benefitted gas capture and separation [32]; the previously delicate (sometimes fragile) and non-easy to handle ZIFs can now be utilised as they come under the purview of a more robust and malleable composite system that offers protection from elevated temperatures and pressures required by practical applications [33,34]. Thus far, the most comprehensive published work dealing with the viability of polymer/MOF composites in the uptake of hydrocarbon is by Bachman et al. [35], who used the combination of M_2 (dobdc) (M = MOF-74 or CPO-27; dobdc = 2,5-dioxido-1,4-benzenedicarboxylate) and 6FDA-DAM to form a composite for C_2H_4 capture. They reported C_2H_4 adsorption values of 3–5 mmol g^{-1} for the original MOFs (powders) while the adsorption capacity of the composites (25 wt% filler) was below 2 mmol g^{-1}. Despite the importance of reversibility in control agents, no desorption studies were reported. The prevalence of other works involving polymer/ZIF composites, or any other form of MOF-based (nano)composites for the reversible uptake of C_2H_4 or any other hydrocarbon, is noticeably absent from literature, with most published works only detailing the viability of MOFs to separate hydrocarbon mixtures [18].

In this study, we focus on the design and characterisation of nano-ZIF/polymer nanocomposites that can achieve reversible C_2H_4 adsorption/desorption at tropical (35 °C) and refrigerated (5 °C) temperatures. We have studied two different classes of polymers for fabricating the nanocomposites: glassy (Matrimid) and rubbery (polyurethane [PU]) matrices that would enable us to contrast the ethylene adsorption–desorption behaviour. Our experimental results show, for the first time, that ZIF nanocrystals encapsulated within polymeric matrices could fully retain their adsorption capability *via* the preservation of their underpinning gate-opening or breathing mechanisms. The adsorption and release kinetics of the ZIF nanocrystals and their corresponding nanocomposites have been carefully evaluated to gain insights into their adsorption/desorption mechanisms, which will prove useful for industrial applications involving hydrocarbon management (for instance, in packaging and transportation of fruits and vegetables).

2. Experimental section

The ZIF-7 and ZIF-8 nanocrystals (nano-ZIFs) were prepared in accordance with methods reported by Cravillon et al. [36] and Li et al. [37] and retained in suspensions of $CHCl_3$ for fabricating the Matrimid/ZIF composites or in tetrahydrofuran (THF) for fabricating the PU/ZIF composites. The chemical structures of the polymers and ZIFs are shown in Fig. S1 in the Supporting Information (SI). The nanocomposites were in turn prepared in accordance with the methods reported by Mahdi et al. [33,38] . Correspondingly, Matrimid flakes and PU beads were dried in a vacuum oven at ~50–60 °C to remove moisture and were then dissolved in their respective solvents ($CHCl_3$ for Matrimid and THF for PU). The polymer solution was then mixed with the aforementioned nanoparticle solutions at a weight ratio of 30 wt%, as per the formula below:

$$\text{ZIF } wt.\% = \left(\frac{m_{\text{ZIF}}}{m_{\text{ZIF}} + m_{\text{polymer}}}\right) \times 100\% \quad (1)$$

The resulting nanocomposite solution was then sonicated, before being casted on a polytetrafluoroethylene (PTFE) substrate at a set thickness of ~100 μm using an automated doctor blade at a speed of 10 mm s^{-1}. The casted nanocomposites were then dried overnight sealed in a glove bag saturated with their respective solvents and then removed the next day to be dried in a vacuum oven at 100 °C for Matrimid and Matrimid-based composites and at 85 °C for PU and PU-based composites.

The textural characterisation of the nanocomposites and the ZIF nanocrystals was performed using N_2 adsorption at cryogenic temperatures. These measurements were performed in a home-built fully automated manometric equipment designed and constructed by the LMA group at Alicante and now commercialised by G2MTech. A total of 100 mg of the samples were sectioned from the nanocomposites, and these were further cut into smaller pieces of 1 mm × 3 mm strips. Prior to the adsorption measurements, all samples were outgassed under UHV conditions (10^{-3} Pa) at 85 °C for 24 h. C_2H_4 measurements were performed in a home-built fully automated manometric equipment, now commercialised by Quantachrome Corp. as VSTAR. C_2H_4 gas adsorption/desorption experiments were performed at temperatures of 5 °C and 35 °C to allow us to study the effects of temperature.

3. Results and discussion

3.1. Characteristics of the synthesised MOF nanocrystals

The morphology of the as-synthesised nanocrystals has been analysed by electron microscopy (Fig. 1). The ZIF-7 nanocrystals appear to be relatively smaller and spherically shaped, with each particle measuring ~30–50 nm, whereas the ZIF-8 nanocrystals are rhombic dodecahedral shaped, with each particle measuring ~150–200 nm. The electron micrographs show a reasonably uniform distribution of the nanoparticles in terms of the size and morphology.

The textural properties of the nanocrystals of ZIF-7 and ZIF-8 being synthesised in this work have been characterised using N_2 adsorption isotherms at −196 °C (77 K). Fig. S2 in the SI shows the characteristic isotherms for both nano-ZIFs. In the specific case of ZIF-8, the N_2 adsorption profile shows the two characteristic steps at p/p_0 ~ 0.005–0.01 and p/p_0 ~ 0.01–0.05, which are associated with the gate-opening effect from the cooperative rotation of the 2-methylimidazolate (mIm) linkers [20–23]. The Brunauer–Emmett–Teller (BET) surface area estimated for ZIF-8 in this

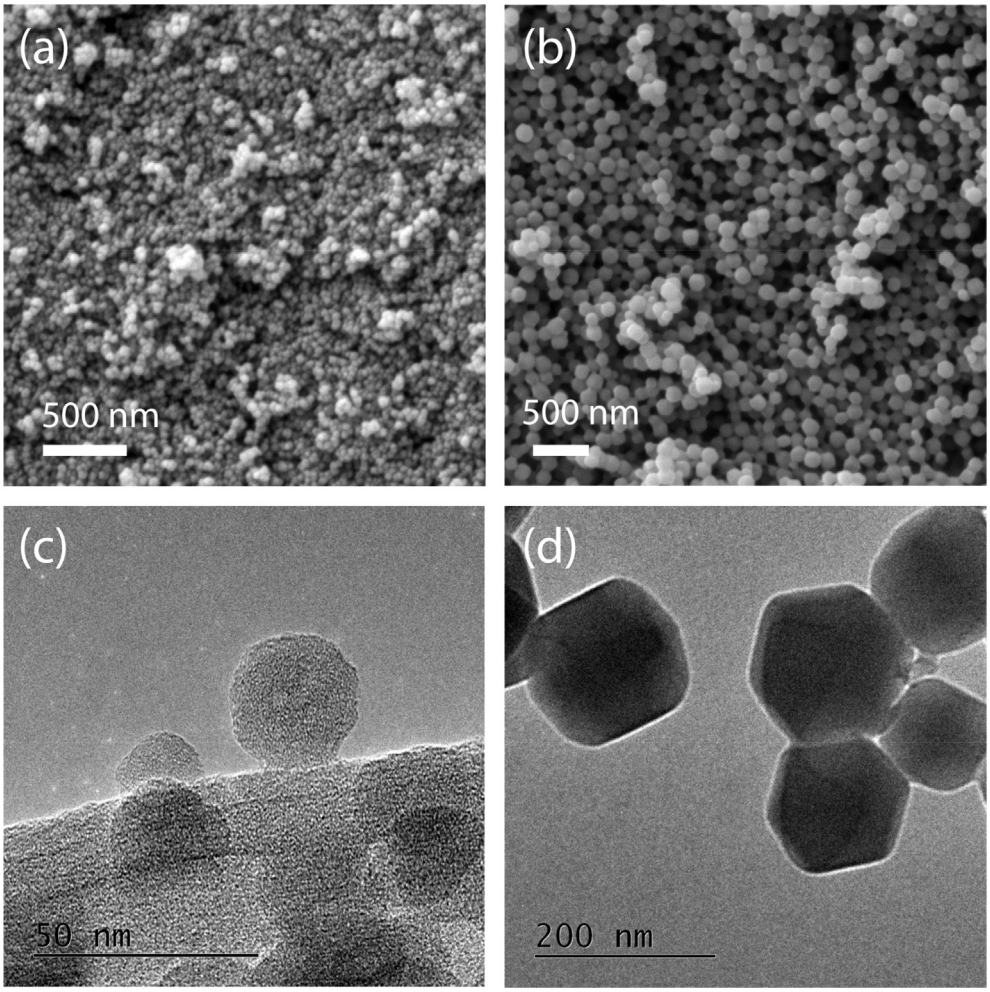

Fig. 1. Electron microscopy (FEG-SEM) images of the nanosized crystals (nanoparticles) of (a) ZIF-7 and (b) ZIF-8 at ~50,000 × magnification. Transmission electron microscope images of individual nanocrystals of (c) ZIF-7 and (d) ZIF-8 taken at ~100,000 × magnification. The mean crystal size of ZIF-7 is ~30–50 nm and that of ZIF-8 is relatively larger, at ~150–200 nm. FEG, field emission gun; SEM, scanning electron microscope; ZIF, zeolitic imidazolate framework.

case is ~1660 $m^2\ g^{-1}$ and its total pore volume is 0.66 $cm^3\ g^{-1}$ [3], which are in close agreement with previous data reported in the literature.

Concerning ZIF-7, recent results detailed by Cuadrado-Collados et al. [25] have shown that it exhibits important kinetic limitations for nitrogen adsorption at cryogenic temperatures. These kinetic restrictions are reflected in the extent of the adsorption measurement because more than a week was required to complete the whole isotherm under strict equilibrium conditions. N_2 adsorption isotherm shows the characteristic multiple steps over the whole pressure range being evaluated, which are associated with the breathing mechanism of the ZIF-7 structure. This is identified as the terahertz vibrational mode [22], where the cooperative deformation of the 2-benzimidazolate (bIm) linkers switches the narrow-pore structure of ZIF-7 (phase II) to an open-pore configuration (phase I) [25,39]. The BET surface area of the as-synthesised ZIF-7 is 264 $m^2\ g^{-1}$, and its total pore volume at p/p_0 ~ 0.97 is ~0.33 $cm^3\ g^{-1}$.

3.2. Characteristics of the fabricated polymer/ZIF nanocomposites

Fig. 2 presents the cross-sectional scanning electron microscope (SEM) images of the polymer matrices and their corresponding polymer/ZIF nanocomposites. SEM images of the cross section of the nanocomposites show that there is a reasonably good dispersion and homogeneity of the nano-ZIFs in the case of both polymer matrices (Matrimid and PU). A comparison between ZIF-7 and ZIF-8 nanocrystals clearly shows that the blending is more effective in the case of ZIF-7, with the nanocrystals being completely embedded within the polymeric matrices (Matrimid and PU). Despite the use of the solution mixing approach [32], we observed some regions showing agglomeration and aggregation of the ZIF-8 nanocrystals, especially in the case of the PU polymer.

The textural properties of the neat polymers and the polymer/ZIF nanocomposites have been evaluated using N_2 adsorption at −196 °C (77 K). As per Fig. S3, the N_2 adsorption capacity for the polymers and their nanocomposites is significantly lower than that for the original nano-ZIFs (18 mmol g^{-1} and 4.8 mmol g^{-1} for ZIF-8 and ZIF-7, respectively, *vs.* < 0.2 mmol g^{-1} for the nanocomposites). It is evident that the adsorption profile is highly oscillatory over the whole relative pressure range evaluated; this fluctuation could be attributed to the mobility of the polymeric chains. However, the presence of additional fluctuations due to the adsorption equipment (e.g., liquid nitrogen level) under this relatively low adsorption conditions cannot be ruled out. The BET surface area estimated for the composites is <1 $m^2\ g^{-1}$, which is quite low compared with that of the nano-ZIFs.

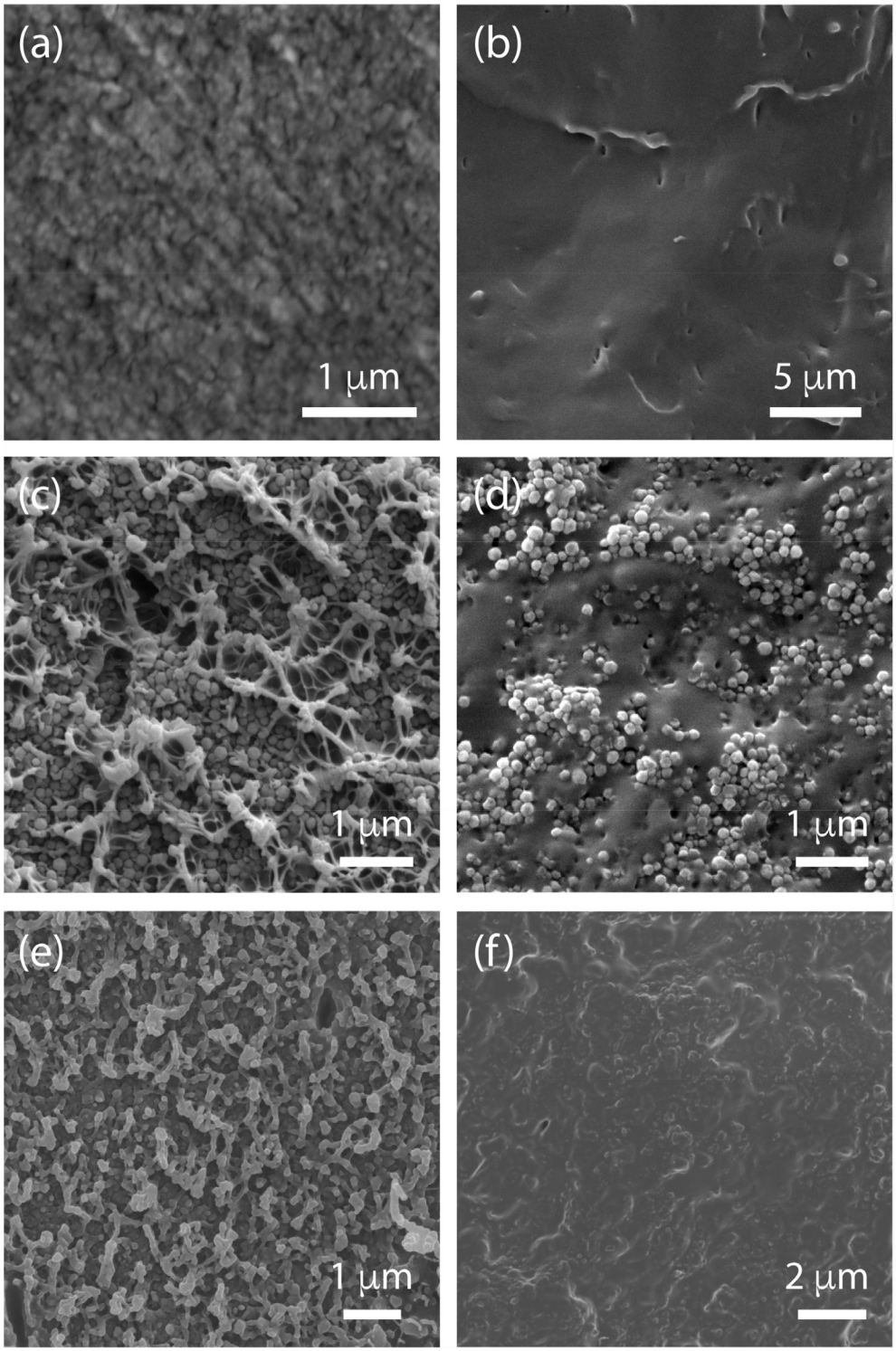

Fig. 2. FEG-SEM images showing the cross sections of the (a) neat Matrimid, (b) neat polyurethane (PU), (c) Matrimid/ZIF-8 30 wt%, (d) PU/ZIF-8 30 wt%, (e) Matrimid/ZIF-7 30 wt%, and (f) PU/ZIF-7 30 wt% at ~50,000 × magnification. FEG, field emission gun; SEM, scanning electron microscope; ZIF, zeolitic imidazolate framework.

3.3. *Ethylene (C_2H_4) adsorption–desorption behaviour*

Fig. 3 shows the ethylene (C_2H_4) adsorption–desorption isotherms of the Matrimid and PU polymer matrices at 5 °C and 35 °C. It can be seen that the adsorption capacity of Matrimid is considerably higher than that of PU, hence revealing an important role of the microstructure of the pristine matrices influencing adsorption. The maximum adsorption capacity of Matrimid stands at ~0.33 mmol g^{-1}, while that of PU was ~0.02 mmol g^{-1} at the same adsorption temperature (5 °C). Following thermodynamics, the adsorption capacity for both matrices are reduced upon an increase in the adsorption temperature; the maximum adsorption capacity of Matrimid at 35 °C was ~0.17 mmol g^{-1}, while that of PU was ~0.01 mmol g^{-1}. Interestingly, while C_2H_4 adsorption in PU is

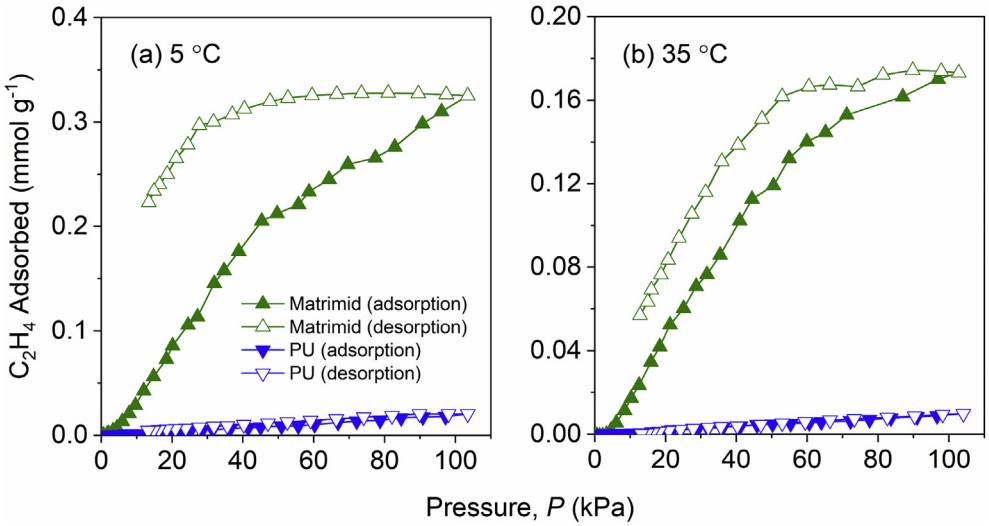

Fig. 3. The adsorption–desorption isotherms of Matrimid and PU polymer matrices measured at (a) 5 °C and (b) 35 °C. The closed and open symbols represent the adsorption and desorption branches of the isotherm, respectively. PU, polyurethane.

completely reversible, Matrimid exhibits a notable hysteresis loop, preferentially at 5 °C. The delay between the adsorption and desorption branch in Matrimid may be attributed to the presence of specific interactions between C_2H_4 and the polymer matrix, as described previously for nitrogen. At this point, it is important to highlight that the large accessibility of C_2H_4 with a kinetic diameter of 0.39 nm to Matrimid at both temperatures exceeded the limited accessibility of N_2, with a smaller kinetic diameter (0.36 nm), at cryogenic temperatures. These observations confirm the presence of a complex adsorption behaviour with important kinetic restrictions in these polymeric matrices, especially at cryogenic temperatures for Matrimid, facilitated by gas–polymer interactions.

The isotherms shown in Fig. 3 (a) and (b) can be explained using the different microstructural characteristic of the two polymers. Matrimid is a polyimide; it is glassy at the experimental temperatures ($T <$ glass transition temperature, T_g), meaning that it has a relatively rigid polymeric configuration (see Fig. S1(a) in SI), providing molecular pathways and improved accessibility to a number of active sites for the formation of hydrogen bonding and weak bonding interactions [33,38,40]. In fact, Matrimid's affinity for alkanes/alkenes has been documented in literature [41,42]. In contrast, PU is a rubbery polymer at the experimental temperatures ($T > T_g$), rendering its more malleable and compliant characteristics thus simpler to manipulate (see Fig. S1(b) in SI) relative to a glassy polymer. Its rubbery nature leads to the poor uptake/retention of C_2H_4 witnessed in the PU sample. The results confirmed that the intrinsic microstructural characteristics of the polymer matrix play a crucial role in the adsorption/desorption of hydrocarbons, and a degree of influence is expected when polymers are used as a matrix to form bespoke polymer nanocomposites (incorporating MOF nanocrystals) for this purpose.

Fig. 4 shows the C_2H_4 adsorption–desorption isotherm plots for the as-synthesised ZIF nanocrystals at the designated adsorption temperatures of 5 °C and 35 °C. Although the crystallographic pore opening (window aperture) of ZIF-7 and ZIF-8 is only 0.29 nm and 0.34 nm, respectively [43], the adsorption isotherm plots clearly show that C_2H_4, with a larger kinetic diameter of 0.39 nm, is able to access the internal porosity (sodalite cage) of both ZIF nanocrystals. However, we observed that the adsorption behaviour for ethylene is completely different despite the similarity in the network composition of both ZIFs (only the imidazolate-type linker differs for ZIF-7 [2-benzimidazolate] and ZIF-8 [2-methylimidazolate]). While the adsorption of C_2H_4 appears to be linear and reversible in the case of ZIF-8 at both adsorption temperatures, ZIF-7 clearly exhibits the breathing phenomenon described previously for N_2 adsorption at cryogenic temperatures [25]. At 5 °C, the breathing phenomena of ZIF-7 takes place in the pressure range of 13.3–33.2 kPa, while this phenomenon has shifted to higher pressures (46.5–73.1 kPa) with the adsorption temperature of 35 °C. At both temperatures, the breathing phenomenon is associated with a hysteresis loop. Contrary to nitrogen where no desorption was observed even at extremely low pressures (Fig. S2), C_2H_4 can desorb from the inner cavities of ZIF-7 (at least partially), thus closing the hysteresis loop. Gücüyener et al. [26] described a similar breathing phenomenon for C_2H_4 in ZIF-7 at pressures ~30–40 kPa for an adsorption temperature of 25 °C, which is in close agreement with our data.

The maximum adsorption capacity of ZIF-8 *vis-à-vis* C_2H_4 at atmospheric pressure (101.3 kPa) exceeds that of ZIF-7 at 5 °C (2.1 mmol g^{-1} vs. 1.4 mmol g^{-1}). The larger adsorption capacity of ZIF-8 vs. ZIF-7 at 5 °C can be attributed to its larger accessible pore volume (solvent accessible volume (SAV) ~ 50% vs. SAV ~26%, respectively) [16]. Increasing the adsorption temperature to 35 °C causes a drop in the total adsorption capacity at atmospheric pressure (101.3 kPa); we found this effect to be more pronounced in the case of ZIF-8. Indeed, ZIF-8 exhibits a decrease in its adsorption capacity by ~54% (2.1 mmol g^{-1} at 5 °C vs. 1 mmol g^{-1} at 35 °C), while the decrease in adsorption capacity detected in ZIF-7 is notably lower, at ~19% (1.4 mmol g^{-1} at 5 °C vs. 1.1 mmol g^{-1} at 35 °C). In other words, our results suggest that the presence of an open structure with a larger mechanical flexibility of ZIF-8 [44] renders it more sensitive to increases in adsorption temperatures relative to the denser ZIF-7, with the latter structure reporting a higher stiffness (Young's modulus, E ~ 6 GPa in ZIF-7 vs. ~ 3 GPa in ZIF-8) [16].

The foregoing sections discussed the adsorption–desorption behaviour of the polymer matrices and the ZIF nanoparticles *vis-à-vis* C_2H_4. The significantly different responses of both types of samples are characteristic of their respective intrinsic structural makeup. However, each type of sample possesses an advantage over another; while the polymers are robust and easily

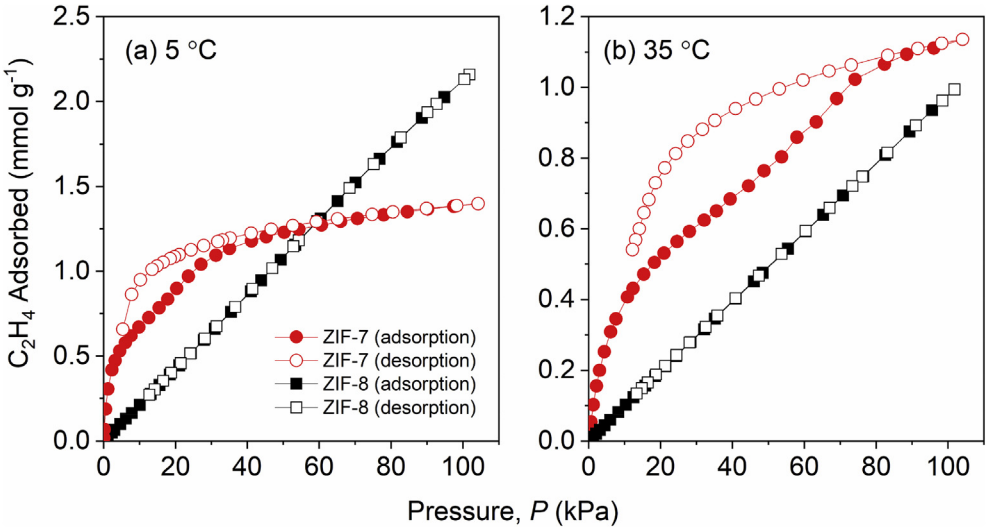

Fig. 4. C_2H_4 adsorption–desorption isotherm plots of the ZIF nanocrystals at (a) 5 °C and (b) 35 °C. ZIF, zeolitic imidazolate framework.

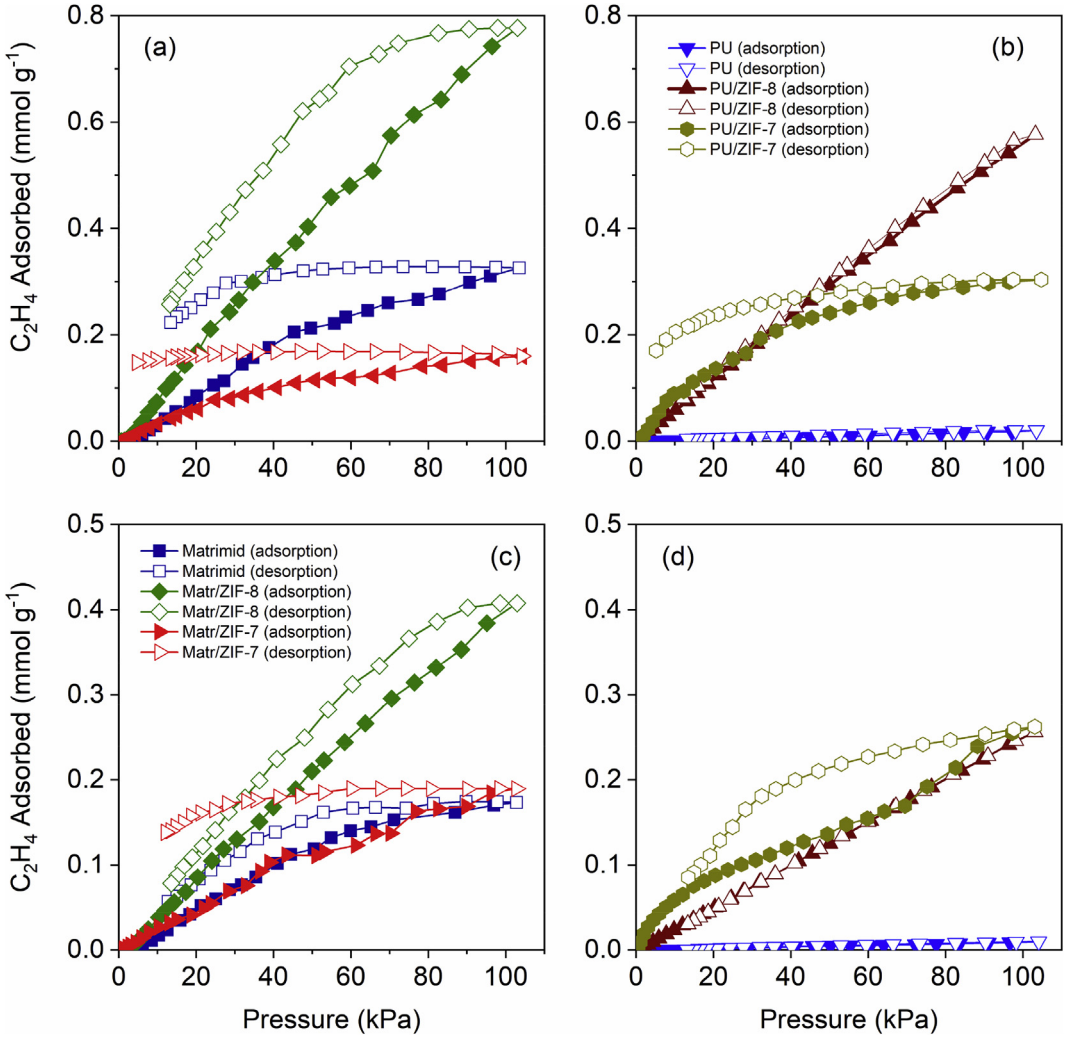

Fig. 5. Adsorption–desorption plots for the polymer/ZIFs nanocomposites, with (a) adsorption–desorption plots for the Matrimid/ZIF nanocomposites at 5 °C, (b) adsorption–desorption plots for the PU/ZIF nanocomposites at 5 °C, (c) adsorption–desorption plots for the Matrimid/ZIF nanocomposites at 35 °C, and (d) adsorption–desorption plots for the PU/ZIF nanocomposites at 35 °C. A compilation of the adsorption/desorption data collated from Figs. 3–5 is presented as an 8-panel plot in Fig. S6 in SI. ZIFs, zeolitic imidazolate frameworks; PU, polyurethane.

customisable despite facing some difficulties adsorbing/desorbing C_2H_4 gas molecules, the ZIF nanocrystals exhibit noticeably higher affinity for the C_2H_4 gas molecules, demonstrating C_2H_4 uptake at levels that are considerably higher than the polymer matrices. In the light of this complementarity, the formation of nanocomposites for the adsorption/desorption of C_2H_4 gas molecules represents the next natural step: the shortcomings presented by both constituents are negated by combining them into one continuous structure. Herein, the low adsorption/desorption of C_2H_4 gas molecules of the polymers is negated by the presence of nano-ZIF nanoparticles (as fillers), as can be seen in Fig. 5.

Bachman et al. [35] described a ~2–3 fold increase in the C_2H_4 adsorption capacity of polyimide 6FDA-DAM after the incorporation of 25 wt% Ni_2(dobdc). A careful evaluation of Fig. 5 (b) & (d) reveals that the adsorption performance in PU-based polymer nanocomposites is dictated by the guest ZIF fillers, i.e. the adsorption isotherm is perfectly linear for ZIF-8 while the breathing of ZIF-7 is evident. Contrarily, in the case of Matrimid-based nanocomposites, a larger contribution from the polymer can be envisaged, including the presence of a large hysteresis loop for all samples, associated with the chemistry and microstructure of the polymeric matrix. A hindered linker distortion in ZIF-8 after its incorporation in Matrimid was also suggested by Diestel et al. [45] to explain the larger H_2/CH_4 selectivity in polymer nanocomposites; this may be attributed to the glassy nature of Matrimid. An increase in the adsorption temperature to 35 °C resulted in a decrease of the adsorption uptake for all samples, except in the case of Matrimid/ZIF-7. A closer look at both polymer-based nanocomposites show that the effect of the adsorption temperature is more important for ZIF-8-based nanocomposites relative to their ZIF-7 counterparts, which is in close agreement with previous data reported for the pristine nano-ZIFs (Fig. 4). In the specific case of Matrimid/ZIF-8, the adsorption uptake decreases by ~47% after an increase in the adsorption temperature (from 5 °C to 35 °C), while its ZIF-7 counterpart does not adhere to thermodynamics by experiencing an increase of ~15% in adsorption capacity. This finding indicates the prevalence of certain kinetic restrictions in the Matrimid-based nanocomposites, at least in the specific case of ZIF-7 as a filler (*vide infra*). In the case of PU-based nanocomposites, an increase in the adsorption temperature (from 5 °C to 35 °C) resulted in a general decrease in the C_2H_4 uptake of ~54% for ZIF-8 and ~13% for ZIF-7. As detailed previously, even at 35 °C, the PU-based nanocomposites exhibit an adsorption performance dictated by the ZIF fillers, while in the Matrimid-based nanocomposites, the glassy matrix exhibits a larger contribution to the adsorption uptake, thus has a greater effect on its overall performance (relative to the PU matrix).

It is important to highlight the fact that the breathing phenomenon of ZIF-7 is perfectly preserved even after being embedded in a polymer matrix, especially in the case of the PU-based nanocomposites. The structural changes (phase transformation) in ZIF-7 composites upon C_2H_4 adsorption at 35 °C takes place at ~60–90 kPa (see Fig. 5(d)), i.e. a pressure slightly shifted to higher values compared to the same phenomenon in the original (unembedded) ZIF. To the best of our knowledge, this is the first experimental evidence confirming the preservation of the dynamic structural phenomena (e.g., gate-opening/breathing mechanism) in ZIFs upon encapsulation in a rubbery polymeric matrix. Significantly, our approach allows for improving the versatility and manipulation of ZIFs while preserving the structural characteristics and accessibility of the ZIFs to hydrocarbon molecules.

As described previously, the polymer nanocomposites contain 30 wt% of ZIFs. According to the adsorption performance of the original ZIFs (see Fig. 4 (a) and (b)), assuming full accessibility of the embedded ZIFs and no contribution from the polymer, the maximum theoretical adsorption capacity for the nanocomposites would be 0.65 mmol g^{-1} and 0.42 mmol g^{-1} for ZIF-8 and ZIF-7 at 5 °C and 0.30 mmol g^{-1} and 0.34 mmol g^{-1} at 35 °C, respectively. In the specific case of PU, the uptake values in the composites are ~11% (for PU/ZIF-8) and ~28% (for PU/ZIF-7) lower than theoretical projections at 5 °C and ~14% (for PU/ZIF-8), and ~23% (for PU/ZIF-7) lower at 35 °C (assuming negligible adsorption from the raw polymer; Fig. 3). These results clearly show the success of our approach with the embedded ZIFs still being highly accessible after being embedded within the PU matrix, i.e. accessibility has been retained at ~90% in the case of ZIF-8 but relatively lower in ZIF-7. In the case of Matrimid, the comparison with the original ZIFs shows that the ZIF-8–based nanocomposite always exceeds theoretical predictions because of the participation of the polymer in the adsorption process. Assuming the adsorption capacity of the raw polymer (Fig. 3) and applying the simple rule of mixtures: contribution $A_{C2H4} = A_{ZIF} \cdot 0.3 + A_{polymer} \cdot 0.7$, we obtain more than 85% accessibility for ZIF-8 in Matrimid (up to ~96% accessibility at 35 °C). However, in the case of the Matrimid/ZIF-7 nanocomposite, the measured adsorption capacity is always below the theoretical predictions, the decrease being much smaller at 35 °C vs. 5 °C (44% vs. 61%), thereby confirming the presence of kinetic restrictions.

Despite the viability of the polymer/MOF nanocomposites in the uptake of C_2H_4 gas molecules, the open question is whether the adsorption performance remains stable after ageing, which is a common concern with polymers. A timed experiment was conducted to interrogate the materials durability; the PU/ZIF-8 and PU/ZIF-7 samples that were used for the adsorption/desorption of C_2H_4 gas molecules in the previous experiment (at 5 °C) were stored after experiment and subjected to the same experiment 3 years later (also at 5 °C). It can be seen in Fig. 6 (a) and (b) that the capability of the PU/ZIF-7 and PU/ZIF-8 nanocomposites to capture/release C_2H_4 gas molecules remained nearly unperturbed by the passage of time (evidenced by the nearly identical plots), confirming its structural stability and undiminished adsorption/desorption capabilities. It is encouraging to see that the linear adsorption/desorption characteristics of the PU/ZIF-8 samples remain stable, with minor deviation after 3 years. This is also evident in the case of the PU/ZIF-7 nanocomposite, which has retained its adsorption/desorption characteristics after 3 years. It can therefore be concluded that the ZIF-7 and ZIF-8 nanoparticles embedded in the nanocomposites remained intact and can be cycled with minimal loss in adsorption capacity. Furthermore, the exposure of the nanocomposite to the high pressures of polarisable gases does not produce any unpredictable loss of capacity because of the plasticisation or polymer swelling (a major obstacle to commercial adoption of polymer nanocomposites) [46]. Our data suggest that the incorporation of ZIF nanoparticles in the polymer matrix could enhance the interactions between the polymeric chains, resulting in improved nanocomposite stability with ageing. Moreover, our recent studies have confirmed that the 30 wt% ZIF/polymer composite systems exhibit an excellent combination of thermomechanical and toughness properties [33,38].

It is critical to understand not only the total adsorption uptake but also the capture/release kinetics of the constituents and the resulting nanocomposites. We evaluated both processes in the synthesised ZIF nanocrystals, where Fig. 7 presents the variation of the pressure in the manifold as a function of equilibrium time for each point of the previously described isotherms, both for the adsorption branch (blue) and the desorption branch (red).

It can be seen in Fig. 7 that the adsorption kinetics for ZIF-8 is an order of magnitude faster compared to ZIF-7. This observation is in close agreement with previous data described in literature for CO_2 and N_2 adsorption for these ZIFs [23,25]. As per Fig. 7(a), while

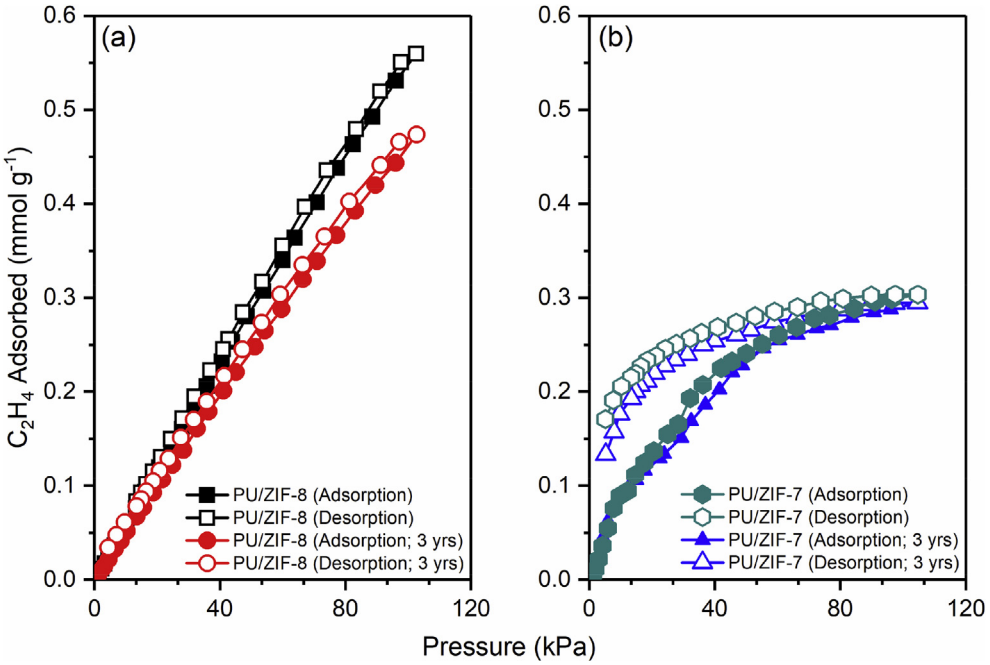

Fig. 6. The adsorption–desorption plots at 5 °C for the current sample and retested after 3 years (a) PU/ZIF-8 nanocomposite and (b) PU/ZIF-7. Test repeatability confirming good materials stability after 3 years. ZIF, zeolitic imidazolate framework; PU, polyurethane.

adsorption/desorption kinetics are more gradual in ZIF-8, the main kinetics limitation for C_2H_4 in ZIF-7 is the breathing phenomena, i.e. the transition from the as-synthesised ZIF-7 narrow-pore phase (phase II) to the open-pore phase (phase I) as depicted in Fig. S5 [39]. The slow kinetics associated with this process can be clearly appreciated both in the adsorption branch (up to 23,000 s for the pore opening) and in the desorption branch (up to 10,000 s are required to switch back from phase I to phase II through the emptying of the pore cavities). Interestingly, these processes become extremely fast (<1000 s) upon an increase in the

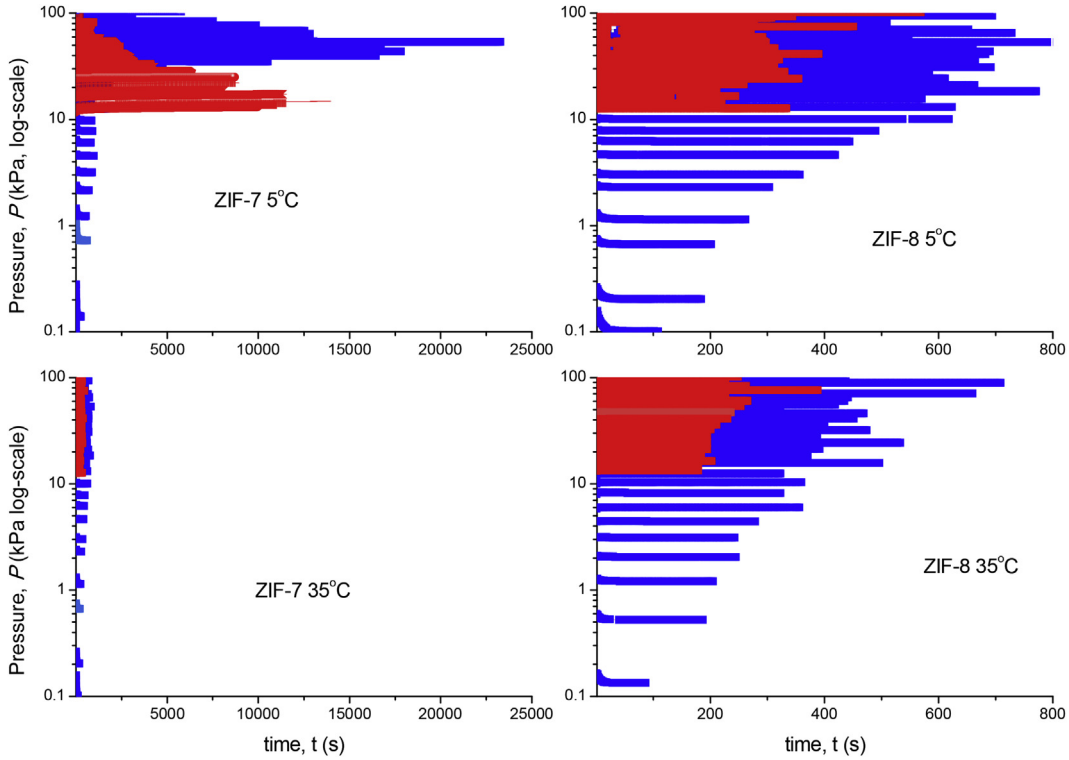

Fig. 7. C_2H_4 adsorption (blue)/desorption (red) kinetics of the ZIF nanoparticles at both experimental temperatures (5 °C and 35 °C) as a function of pressure (log-scale) and time. ZIF, zeolitic imidazolate framework.

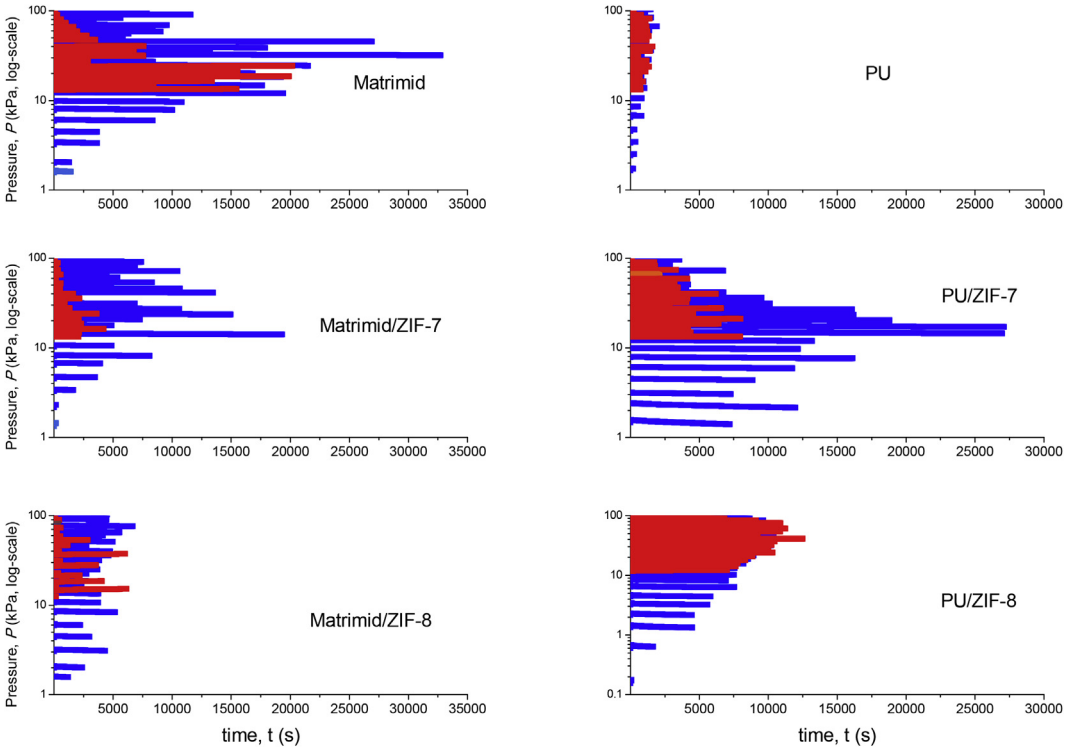

Fig. 8. C_2H_4 adsorption (blue)/desorption (red) kinetics of the polymer matrices (Matrimid and PU) and their corresponding ZIF-(7&8) nanocomposite samples at the experimental temperature of 5 °C as a function of pressure (log-scale) and time. ZIF, zeolitic imidazolate framework; PU, polyurethane.

adsorption temperature from 5 °C to 35 °C, at which the adsorption and desorption kinetics become comparable to those of ZIF-8.

The adsorption/desorption kinetics are shown in Fig. 8, summarising the data of the polymer matrices and their corresponding ZIF-(7&8) nanocomposite samples at 5 °C. It can be seen in Fig. 8(a) that despite Matrimid having a higher affinity for hydrocarbons relative to PU, this higher adsorption uptake is associated with very slow kinetics. The incorporation of ZIF nanofillers in Matrimid resulted, in both cases, in the improvements of the adsorption and desorption kinetics (desorption is notably fast in these nanocomposites); these effects being most prominent by embedding the ZIF-8 fillers. Remarkably, the scenario is reversed in the case of PU-based nanocomposites. In this case, the incorporation of the nanofillers slows down the adsorption and desorption kinetics, preferentially in the case of ZIF-7 because of the breathing phenomenon. Notably, the PU/ZIF-8 nanocomposite exhibits slightly larger kinetics for the desorption branch compared to the adsorption branch.

The desorption of ethylene in ZIF-7/polymer composites is relatively faster than that in ZIF-8/polymer nanocomposites. This is because while in ZIF-8–based samples the desorption takes place already from the beginning of the desorption branch (at 1 bar, see Fig. 4), in the ZIF-7–based samples, the desorption is delayed down in pressure because of the breathing effect. Once desorption takes place, it becomes faster because of thermodynamics. However, it is also true that the desorption is not complete as it can be appreciated in Fig. 5, i.e. some ethylene remains trapped in the phase-II structure of ZIF-7. This is also the case for the original ZIFs shown in Fig. 4.

Finally, it should be noted that the data presented in Figs. 7 and 8 are not direct kinetics because of the configuration of the current manifold setup (these measurements report the pressure decay at the manifold until equilibrium is reached at each point of the isotherm, the manifold pressure being expanded to a sample cell already filled with gas from the previous adsorption measurement); however, these qualitative results are very useful for pinpointing the breathing phenomenon of ZIF-7 and its polymer/ZIF composites as demonstrated in this study.

4. Conclusions

This research demonstrates the tuneable capacity of polymer/nano-ZIFs composites to control the adsorption/desorption of C_2H_4 gas molecules *via* common external factors such as temperatures and pressures. We established that the neat polymer matrices (Matrimid and PU) are limited in their capability for the uptake and release of C_2H_4 gas molecules, but with the addition of ZIF-(7&8) nanoparticles as porous functional fillers (both with high affinity for hydrocarbons), the resulting nanocomposites could improve the material performance (i.e. from nearly negligible adsorption/desorption by the polymers to an average of ~0.5 mmol g^{-1} adsorption/desorption for the polymer/ZIF nanocomposites at 5 °C and 35 °C) because of the preservation of the intrinsic properties of the ZIF nanocrystals within the polymer matrices. On the role of the polymer matrix, it provides a continuous medium to encapsulate the nanosized ZIF crystals so that it can be deployed for practical applications. The polymer matrix also offers support to enhance mechanical stability when exposed to temperatures and humidity because some MOFs can be temperature or water sensitive.

It was also established that the inclusion of ZIF nanoparticles within the polymer matrix generates a trapping effect, which effectively suppresses the desorption of the C_2H_4 gas molecules to a level that makes it possible for the process to be manipulated by a combination of external pressure and temperature stimuli. These results open the door towards the application of novel ZIF–polymer

nanocomposites for industrial applications such as packaging and transportation of fruits and vegetables, where a precise control of C_2H_4 in the gas phase is important for controlled ripening of perishable produce [47–49]. Future work is warranted to pinpoint the precise adsorption mechanisms in polymer/ZIF nanocomposites responsible for the adsorption/desorption of C_2H_4.

Declaration of interests

The authors declare that they have no known competing financial interests or personal relationships that could have appeared to influence the work reported in this paper.

Acknowledgements

E. M. Mahdi would like to thank Yayasan Khazanah (YK) for the DPhil scholarship that made this work possible. The research in the MMC Lab (J.C.T.) was supported by the European Research Council (ERC) under the European Union's Horizon 2020 research and innovation programme (grant agreement No 771575 - PROMOFS), and the EPSRC grant no. EP/N014960/1. The authors acknowledge the provision of the TGA and TEM by the Research Complex at Harwell (RCaH), in Rutherford Appleton Laboratory, Oxfordshire. J.S.A. acknowledges financial support by MINECO (Project MAT2016-80285-p), H2020 (MSCA-RISE-2016/NanoMed Project), and GV (PROMETEOII/2014/004).

Appendix A. Supplementary data

Supplementary data to this article can be found online at https://doi.org/10.1016/j.mtadv.2019.100008.

References

[1] Global horticulture assessment. https://pdf.usaid.gov/pdf_docs/Pnadh769.pdf (accessed May 2018).
[2] The food and agriculture organization (FAO) of the united nations. http://www.fao.org/save-food/en/(accessed May 2018).
[3] A.H. Tullo, AgroFresh invests in ethylene removal, Chem. Eng. News 96 (2018) 12.
[4] A.L. Brody, E.R. Strupinsky, L.R. Kline, Active Packaging for Food Applications, CRC Press, USA, 2001.
[5] N. Pathak, O.J. Caleb, M. Geyer, W.B. Herppich, C. Rauh, P.V. Mahajan, Photocatalytic and photochemical oxidation of ethylene: potential for storage of fresh produce — a review, Food Bioprocess Technol. 10 (2017) 982–1001.
[6] M.L. Rooney, Active Food Packaging, Springer, USA, 1995.
[7] K. Takahashi, T. Motodate, K. Takaki, S. Koide, Influence of oxygen concentration on ethylene removal using dielectric barrier discharge, Jpn. J. Appl. Phys. 57 (2018) 01AG04.
[8] H. Bodaghi, Y. Mostofi, A. Oromiehie, B. Ghanbarzadeh, Z.G. Hagh, Synthesis of clay-TiO_2 nanocomposite thin films with barrier and photocatalytic properties for food packaging application, J. Appl. Polym. Sci. 132 (2015) 41764.
[9] S.D.F. Mihindukulasuriya, L.T. Lim, Nanotechnology development in food packaging: a review, Trends Food Sci. Technol. 40 (2014) 149–167.
[10] J.-R. Li, Y. Ma, M.C. McCarthy, J. Sculley, J. Yu, H.-K. Jeong, P.B. Balbuena, H.-C. Zhou, Carbon dioxide capture-related gas adsorption and separation in metal-organic frameworks, Coord. Chem. Rev. 255 (2011) 1791–1823.
[11] S.J. Geier, J.A. Mason, E.D. Bloch, W.L. Queen, M.R. Hudson, C.M. Brown, J.R. Long, Selective adsorption of ethylene over ethane and propylene over propane in the metal-organic frameworks M_2(dobdc) (M = Mg, Mn, Fe, Co, Ni, Zn), Chem. Sci. 4 (2013) 2054–2061.
[12] Y. Zhang, B. Li, R. Krishna, Z. Wu, D. Ma, Z. Shi, T. Pham, K. Forrest, B. Space, S. Ma, Highly selective adsorption of ethylene over ethane in a MOF featuring the combination of open metal site and pi-complexation, Chem. Commun. 51 (2015) 2714–2717.
[13] S. Chavan, F. Bonino, J.G. Vitillo, E. Groppo, C. Lamberti, P.D. Dietzel, A. Zecchina, S. Bordiga, Response of CPO-27-Ni towards CO, N_2 and C_2H_4, Phys. Chem. Chem. Phys. 11 (2009) 9811–9822.
[14] X. Cui, K. Chen, H. Xing, Q. Yang, R. Krishna, Z. Bao, H. Wu, W. Zhou, X. Dong, Y. Han, et al., Pore chemistry and size control in hybrid porous materials for acetylene capture from ethylene, Science 353 (2016) 141–144.
[15] K.S. Park, Z. Ni, A.P. Cote, J.Y. Choi, R.D. Huang, F.J. Uribe-Romo, H.K. Chae, M. O'Keeffe, O.M. Yaghi, Exceptional chemical and thermal stability of zeolitic imidazolate frameworks, Proc. Natl. Acad. Sci. U.S.A. 103 (2006) 10186–10191.
[16] J.C. Tan, T.D. Bennett, A.K. Cheetham, Chemical structure, network topology, and porosity effects on the mechanical properties of zeolitic imidazolate frameworks, Proc. Natl. Acad. Sci. U.S.A. 107 (2010) 9938–9943.
[17] K. Li, D.H. Olson, J. Seidel, T.J. Emge, H. Gong, H. Zeng, J. Li, Zeolitic imidazolate frameworks for kinetic separation of propane and propene, J. Am. Chem. Soc. 131 (2009) 10368–10369.
[18] Z. Bao, G. Chang, H. Xing, R. Krishna, Q. Ren, B. Chen, Potential of microporous metal-organic frameworks for separation of hydrocarbon mixtures, Energy Environ. Sci. 9 (2016) 3612–3641.
[19] Y. Pan, Z. Lai, Sharp separation of C_2/C_3 hydrocarbon mixtures by zeolitic imidazolate framework-8 (ZIF-8) membranes synthesized in aqueous solutions, Chem. Commun. 47 (2011) 10275–10277.
[20] D. Fairen-Jimenez, S.A. Moggach, M.T. Wharmby, P.A. Wright, S. Parsons, T. Duren, Opening the gate: framework flexibility in ZIF-8 explored by experiments and simulations, J. Am. Chem. Soc. 133 (2011) 8900–8902.
[21] C.O. Ania, E. Garcia-Perez, M. Haro, J.J. Gutierrez-Sevillano, T. Valdes-Solis, J.B. Parra, S. Calero, Understanding gas-induced structural deformation of ZIF-8, J. Phys. Chem. Lett. 3 (2012) 1159–1164.
[22] M.R. Ryder, B. Civalleri, T.D. Bennett, S. Henke, S. Rudić, G. Cinque, F. Fernandez-Alonso, J.C. Tan, Identifying the role of terahertz vibrations in metal-organic frameworks: from gate-opening phenomenon to shear-driven structural destabilization, Phys. Rev. Lett. 113 (2014) 215502.
[23] M.E. Casco, Y.Q. Cheng, L.L. Daemen, D. Fairen-Jimenez, E.V. Ramos-Fernandez, A.J. Ramirez-Cuesta, J. Silvestre-Albero, Gate-opening effect in ZIF-8: the first experimental proof using inelastic neutron scattering, Chem. Commun. 52 (2016) 3639–3642.
[24] S. Aguado, G. Bergeret, M.P. Titus, V. Moizan, C. Nieto-Draghi, N. Bats, D. Farrusseng, Guest-induced gate-opening of a zeolite imidazolate framework, New J. Chem. 35 (2011) 546–550.
[25] C. Cuadrado-Collados, J. Fernandez-Catala, F. Fauth, Y.Q.Q. Cheng, L.L. Daemen, A.J. Ramirez-Cuesta, J. Silvestre-Albero, Understanding the breathing phenomena in nano-ZIF-7 upon gas adsorption, J. Mater. Chem. A 5 (2017) 20938–20946.
[26] C. Gücüyener, J. van den Bergh, J. Gascon, F. Kapteijn, Ethane/ethene separation turned on its head: selective ethane adsorption on the metal-organic framework ZIF-7 through a gate-opening mechanism, J. Am. Chem. Soc. 132 (2010) 17704–17706.
[27] H. Bux, C. Chmelik, R. Krishna, J. Caro, Ethene/ethane separation by the MOF membrane ZIF-8: molecular correlation of permeation, adsorption, diffusion, J. Membr. Sci. 369 (2011) 284–289.
[28] U. Bohme, B. Barth, C. Paula, A. Kuhnt, W. Schwieger, A. Mundstock, J. Caro, M. Hartmann, Ethene/ethane and propene/propane separation via the olefin and paraffin selective metal-organic framework adsorbents CPO-27 and ZIF-8, Langmuir 29 (2013) 8592–8600.
[29] E.M. Mahdi, J.C. Tan, Metal–organic framework based composites, in: P.W.R. Beaumont, C.H. Zweben (Eds.), Comprehensive Composite Materials II, vol. 4, Academic Press, Oxford, 2018, pp. 525–553.
[30] Y.V. Kaneti, S. Dutta, M.S.A. Hossain, M.J.A. Shiddiky, K.L. Tung, F.K. Shieh, C.K. Tsung, K.C.W. Wu, Y. Yamauchi, Strategies for improving the functionality of zeolitic imidazolate frameworks: tailoring nanoarchitectures for functional applications, Adv. Mater. 29 (2017) 1700213.
[31] B. Zornoza, C. Tellez, J. Coronas, J. Gascon, F. Kapteijn, Metal organic framework based mixed matrix membranes: an increasingly important field of research with a large application potential, Microporous Mesoporous Mater. 166 (2013) 67–78.
[32] Q. Song, S.K. Nataraj, M.V. Roussenova, J.C. Tan, D.J. Hughes, W. Li, P. Bourgoin, M.A. Alam, A.K. Cheetham, S.A. Al-Muhtaseb, et al., Zeolitic imidazolate framework (ZIF-8) based polymer nanocomposite membranes for gas separation, Energy Environ. Sci. 5 (2012) 8359–8369.
[33] E.M. Mahdi, J.C. Tan, Mixed-matrix membranes of zeolitic imidazolate framework (ZIF-8)/Matrimid nanocomposite: thermo-mechanical stability and viscoelasticity underpinning membrane separation performance, J. Membr. Sci. 498 (2016) 276–290.
[34] J. Dechnik, C.J. Sumby, C. Janiak, Enhancing mixed-matrix membrane performance with metal–organic framework additives, Cryst. Growth Des. 17 (2017) 4467–4488.
[35] J.E. Bachman, Z.P. Smith, T. Li, T. Xu, J.R. Long, Enhanced ethylene separation and plasticization resistance in polymer membranes incorporating metal-organic framework nanocrystals, Nat. Mater. 15 (2016) 845–849.
[36] J. Cravillon, S. Münzer, S.J. Lohmeier, A. Feldhoff, K. Huber, M. Wiebcke, Rapid room-temperature synthesis and characterization of nanocrystals of a prototypical zeolitic imidazolate framework, Chem. Mater. 21 (2009) 1410–1412.
[37] Y.S. Li, F.Y. Liang, H. Bux, A. Feldhoff, W.S. Yang, J. Caro, Molecular sieve membrane: supported metal-organic framework with high hydrogen selectivity, Angew. Chem. Int. Ed. 49 (2010) 548–551.
[38] E.M. Mahdi, J.C. Tan, Dynamic molecular interactions between polyurethane and ZIF-8 in a polymer-MOF nanocomposite: microstructural, thermo-mechanical and viscoelastic effects, Polymer 97 (2016) 31–43.

[39] P. Zhao, G.I. Lampronti, G.O. Lloyd, M.T. Wharmby, S. Facq, A.K. Cheetham, S.A.T. Redfern, Phase transitions in zeolitic imidazolate framework 7: the importance of framework flexibility and guest-induced instability, Chem. Mater. 26 (2014) 1767–1769.
[40] S.J.K. Jensen, T.H. Tang, I.G. Csizmadia, Hydrogen-bonding ability of a methyl group, J. Phys. Chem. A 107 (2003) 8975–8979.
[41] C.A. Scholes, W.X. Tao, G.W. Stevens, S.E. Kentish, Sorption of methane, nitrogen, carbon dioxide, and water in Matrimid 5218, J. Appl. Polym. Sci. 117 (2010) 2284–2289.
[42] F. Falbo, A. Brunetti, G. Barbieri, E. Drioli, F. Tasselli, CO2/CH4 separation by means of Matrimid hollow fibre membranes, App. Pet. Res. 6 (2016) 439–450.
[43] A. Phan, C.J. Doonan, F.J. Uribe-Romo, C.B. Knobler, M. O'Keeffe, O.M. Yaghi, Synthesis, structure and carbon dioxide capture properties of zeolitic imidazolate frameworks, Acc. Chem. Res. 43 (2010) 58–67.
[44] J.C. Tan, B. Civalleri, C.C. Lin, L. Valenzano, R. Galvelis, P.F. Chen, T.D. Bennett, C. Mellot-Draznieks, C.M. Zicovich-Wilson, A.K. Cheetham, Exceptionally low shear modulus in a prototypical imidazole-based metal-organic framework, Phys. Rev. Lett. 108 (2012) 095502.
[45] L. Diestel, N. Wang, B. Schwiedland, F. Steinbach, U. Giese, J. Caro, MOF based MMMs with enhanced selectivity due to hindered linker distortion, J. Membr. Sci. 492 (2015) 181–186.
[46] G. Dong, H. Li, V. Chen, Challenges and opportunities for mixed-matrix membranes for gas separation, J. Mater. Chem. A 1 (2013) 4610–4630.
[47] S. Ahmad, A.K. Thompson, Effect of controlled atmosphere storage on ripening and quality of banana fruit, J. Hortic. Sci. Biotechnol. 81 (2006) 1021–1024.
[48] H.J.D. Lalel, Z. Singh, Controlled atmosphere storage of 'Delta R2E2' mango fruit affects production of aroma volatile compounds, J. Hortic. Sci. Biotechnol. 81 (2006) 449–457.
[49] World's first commercial MOF keeps fruit fresh. https://www.chemistryworld.com/news/worlds-first-commercial-mof-keeps-fruit-fresh/1017469.article (accessed April 2018).